Proceedings of CECNet 2022
A.J. Tallón-Ballesteros (Ed.)

doi:10.3233/FAIA220557

Spin Sensitivity and Magnetic Response Analysis of Nano-SQUIDs

Zejun SHI [a,b], Huachuan WANG* [a,b] and Jianxin LIN* [a,b]

[a] *Qingdao Innovation and Development Center of Harbin Engineering University, Qingdao, 266404, China*

[b] *College of Intelligent Systems Science and Engineering, Harbin Engineering University, Harbin 150001, China*

Abstract. This paper presents the spin sensitivity and magnetic response analysis of the nano-superconducting-quantum-interference devices (SQUIDs). We employed the computational study to understand the schemes of a nano-SQUID's detection capability according to the device's geometry and fabrication process. We find that the performance of the nano-device increased by decreasing the loop size of the SQUIDs, and it reached the maximum value at the corners of the loop. We then estimated the flux noise S_Φ of the SQUIDs in the thermal white noise regime and discussed the field amplification factor around the cross-section area. Furthermore, we fabricated $YBa_2Cu_3O_7$ (YBCO) based nano-SQUIDs with Josephson junctions at MgO biocrystal grain boundaries using the Pulsed Laser Deposition (PLD) and Focused Ion Beam (FIB) technique. By comparison with the estimated value of our calculation, the spin sensitivity evaluated by the experimentally fabricated devices coincides nicely with our estimation.

Keywords. Josephson junction,nanoSQUIDs,simulation,spin sensitivity,microfluidic technology

1. Introduction

Superconducting quantum interference devices (SQUIDs) with direct current (dc) are promising sub-micrometer dimension devices for probing quantum physical systems [1,2], such as small spin systems[3,4] and high sensitivity magnetometry[5]. High-temperature SQUID does not require expensive cryogenic refrigeration equipment, thus more capable as the building block for modern nanoscale applications [6,7,8,9].

A $YBa_2Cu_3O_7$ (YBCO) dc SQUID constitutes a thin film superconducting loop, and Josephson junctions interrupt the loop. It converts the magnetic flux into current or voltage. When the current is more extensive than the Josephson critical current I_0, the junction switches to a resistive state, and the device's voltage will no longer remain zero due to the cooper pair-tunneling through the junction, shown in Figure. 1. A SQUID with high sensitivity can detect any form of energy that can convert into magnetic flux

*Corresponding Author
hcwang@hrbeu.edu.cn
linjianxin@hrbeu.edu.cn

within the loop of the SQUID. Recently, extremely low spin spectral density within the range of hundred nanometers has been reported[8,9]. The SQUID's sensitivity depends strongly on the device's design[10]. To increase the SQUIDs' detecting performance, the magnetic moment down to a single spin level, optimizing the SQUID's design to fabricate an appropriate SQUID sensor is necessary.

Simulation studies of a magnetic nanoparticle at any generic position above the SQUID loop and the corresponding influence to the magnetic flux were reported recently by Granata[2], Tilbrook[11] and Bouchiat[7]. The spin sensitivity of a SQUID layout is $S_\mu^{1/2} = S_\Phi^{1/2}/\Phi_\mu$ [12], in this function S_Φ is the magnetic flux noise and Φ_μ is the coupling factor. Given that the level of the inductance of the SQUID L is proportional to the magnetic flux noise S_Φ, it is necessary for us to reduce the inductance in order to increase the sensitivity [6,13]. In order to decrease the inductance, the dimension of the SQUID loop has to be reduced to submicron size. The details of the magnetic coupling between the SQUID device and the single spin need to be studied to predict the response of the SQUID corresponding to a single spin located at different positions within the device[14]. Moreover, this study can provide more perspectives regarding optimizing the SQUID single spin sensor [15].

This paper reports the detailed evaluation process of the SQUID's sensitivity and response relative to the single spin as a function of position within the SQUID loop. We then fabricated YBCO-based nano-SQUIDs with Josephson junctions at MgO biocrystal grain boundaries using the Pulsed Laser Deposition (PLD) and Focused Ion Beam (FIB) technique [16]. The electrical current, magnetic voltage, and noise are measured under liquid nitrogen temperature in an electrically and magnetically shielded environment to characterize the device's properties.

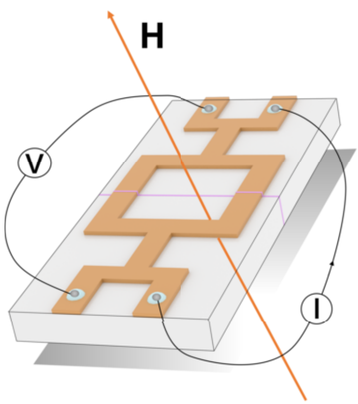

Figure 1. Schematic of the magnetic field passing through nanoSQUIDs.

2. Methodology

2.1. Spin sensitivity computation

To evaluate the spin sensitivity $S_\mu^{1/2}$ of the SQUID device, we need to know the coupling factor Φ_μ between the spin and SQUID [17]. Let us consider a single spin

($\mu_B = 9.3 \times 10\exp{-24J/T}$) oriented along the z-axis, positioned within a rectangular geometry SQUID whose side length is a and width is b (shown in Figure. 2). The spin located at $P(x', y', z')$. Because the magnetic flux of the spin in the SQUID loop's direction does not contribute to the magnetic threading of the loop. The surface integral of the magnetic field threading by the magnetic moment μ_B over the loop is equal to the path integral of the potential vector of the spin tracing the loop of the SQUID, shown in Equation (5)

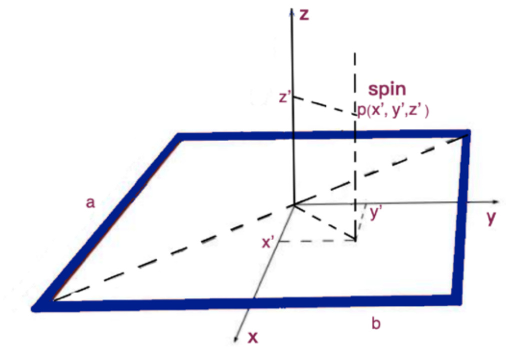

Figure 2. A spin located at a generic position within the SQUID loop.

$$\Phi_\mu = \oint \mathbf{A}(\mathbf{r}) \cdot d\mathbf{s} \tag{1}$$

Where $\mathbf{A}(\mathbf{r})$ is the magnetic vector potential. The x and y direction components of the magnetic vector potential at generic position $P(x', y', z')$ along the z-axis are [8],

$$\begin{aligned} A_x &= -\frac{\mu_0\mu_B}{4\pi}\frac{y}{\mathbf{r}^3} \\ A_y &= \frac{\mu_0\mu_B}{4\pi}\frac{x}{\mathbf{r}^3} \end{aligned} \tag{2}$$

Where $\mathbf{r}$ is the distance between the spin and the plan of the SQUID loop, and μ_0 is the magnetic vacuum permeability. The magnetic flux of a spin as a function of its position within the loop is,

$$\begin{aligned} \Phi_\mu(x', y', z') = -\frac{\mu_0\mu_B}{4\pi}\Big(&\int_{-\frac{b}{2}}^{\frac{b}{2}} \frac{(a/2 - x')}{\mathbf{r}^3}dy + \int_{\frac{a}{2}}^{-\frac{a}{2}} \frac{(b/2 - y')}{\mathbf{r}^3}dx \\ &+ \int_{\frac{b}{2}}^{-\frac{b}{2}} \frac{(-a/2 - x')}{\mathbf{r}^3}dy + \int_{-\frac{a}{2}}^{\frac{a}{2}} \frac{(-b/2 - y')}{\mathbf{r}^3}dx\Big) \end{aligned} \tag{3}$$

We further expand the above Equation (Equation 2.1) and revised the Equation as below,

$$\begin{aligned}\Phi_\mu(x',y',z') = -\frac{\mu_0\mu_B}{4\pi}\Big(&\int_{-\frac{b}{2}}^{\frac{b}{2}} \frac{\frac{a}{2}-x'}{[((a/2-x')')^2+(y-y')^2+z'^2]^{3/2}}dy \\ &+\int_{\frac{a}{2}}^{-\frac{a}{2}} \frac{\frac{b}{2}-y'}{[((x-x')')^2+(b/2-y')^2+z'^2]^{3/2}}dx \\ &+\int_{\frac{b}{2}}^{-\frac{b}{2}} \frac{-\frac{a}{2}-x'}{[((-a/2-x')')^2+(y-y')^2+z'^2]^{3/2}}dy \\ &+\int_{-\frac{a}{2}}^{\frac{a}{2}} \frac{-\frac{b}{2}-y'}{[((x-x')')^2+(-b/2-y')^2+z'^2]^{3/2}}dx\Big)\end{aligned} \tag{4}$$

2.2. Magnetic flux noise

The other most critical factor of a SQUID device is the magnetic flux noise. We use the theoretical expression from Langevin simulations to determine the flux noise of the SQUID in the thermal white noise regime [18,19,20,21],

$$S_\Phi = f(\beta_L)\Phi_0 k_B T L/I_0 R \tag{5}$$

Here, the β_L is the screening parameter, I_0 is the critical current, and L is the inductance. For lower values of β_L, S_Φ increases. Furthermore, it is important to notice from this Equation that $S_\Phi \propto L$. The decreasing inductance will reduce the flux noise. We know that L will decrease with the contribution of miniaturization of the SQUID loop size and increase the thickness of the $YBCO$superconducting film, which means S_Φ is linearly dependent on the side length and film thickness of the SQUID.

2.3. Field amplification factor around the cross-section area

In this section, we discuss the magnetic amplification effect around the SQUID loop's cross-section area (constriction or junctions). The layout of the nanoSQUID (top view) is shown in Figure. 3(a). As shown in Figure. 3 (b), a and b are the width and thickness of the cross-section, respectively, d is the length of the constriction, λ is the London penetration depth, x and y are the widths, and the thickness direction of the cross-section, and z is the length direction of the cross-section [8,4]. Magnetic flux density at the x direction over the cross-section with a rectangular cross-section can be calculated using the Biot–Savart law.

$$B_x(x',y',z') = -\frac{\mu_0}{4\pi}\int_0^b\int_0^a\int_{-d/2}^{d/2}\frac{(y'-y)j(x)}{\mathbf{r}^3}dxdydz \tag{6}$$

Where $j(x)$he distribution of shielding current, $j(x,y) = j(x) = \frac{1}{2\lambda b}e^{(|x|-a)/\lambda}$.

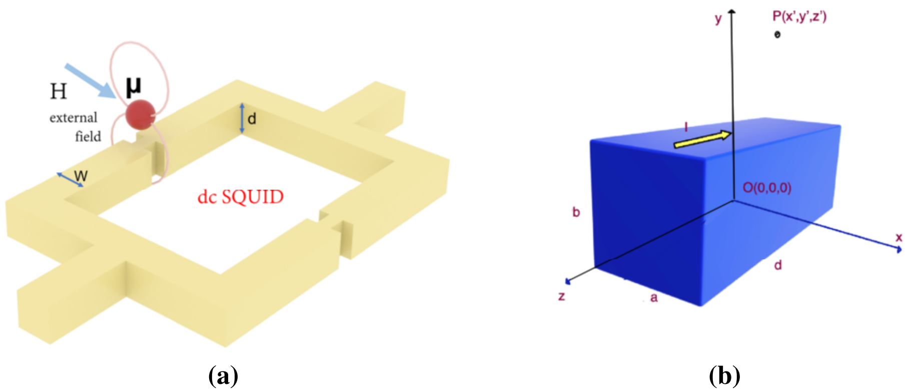

Figure 3. **(a)** Schematic diagram of magnetic nanoparticles on top of the cross-section area of a nanoSQUID. **(b)** Schematic diagram of the structure and coordinate systems of the cross-section area.

3. Results

Solving the analytically expressed Equation (2.1) numerically, we obtained the magnetic flux produced by a single spin as a function of its position within the SQUID loop. Figure. 4 reports the magnetic flux distribution of a single spin at the *xy*-plane, 10*nm* above the SQUID loop. The side length of the SQUID loop is a = 380 nm and b = 220. The highest values of the magnetic flux are obtained when the spin is close to the corner of the loop, as is shown in Figure. 4,.

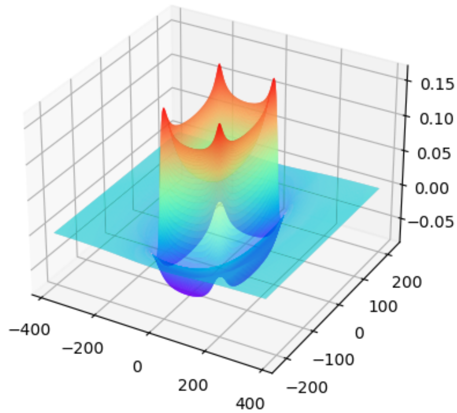

Figure 4. Distribution of the magnetic flux produced by a single spin within the SQUID loop. The side length of the loop is $a = 380nm$ and $b = 220nm$. The distance of between the spin and loop's xy-plane is $z' = 10nm$.

By modifying the distance z' value between the spin and the xy-plane of the SQUID loop, we find the dependence in the Equation within $-100nm \leq z \leq 100nm$ with abso-

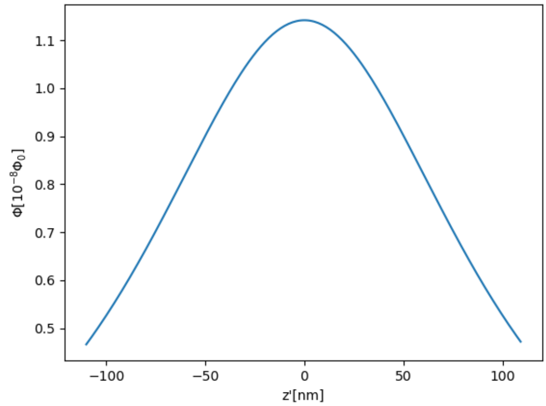

Figure 5. Calculating the coupling factor in the range of $-100nm \leq z \leq 100nm$.

lute values scaling like $\Phi_\mu \propto z^{-3/2}$, shown in Figure. 5. Decreasing z direction distance towards the SQUID loop, the values of the magnetic flux increase.

Figure. 6 (a) and (b) show the amplification factor variant along the x-direction. By reducing the width of the cross-section from $50nm$ to $10nm$, the maximum amplification factor continuously increases. However, when the width of the cross-section area decreased, the peak of the amplification factor gradually transformed from two peaks on both sides to one peak at the center of the cross-section area. Meanwhile, the peak value of the amplification factor becomes larger. This result indicates that, in order to enhance the sensitivity of the nano-SQUID devices, the particle under test should be positioned above the center of the cross-section of the SQUID loop.

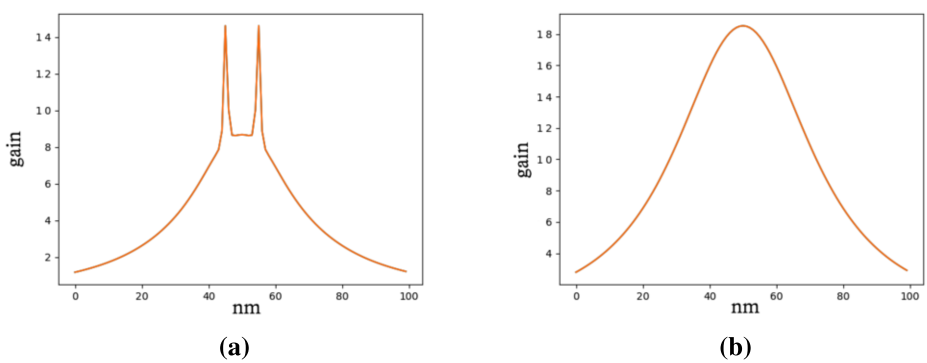

Figure 6. Field amplification factor distribution along the width direction of the cross-section. The distance above the SQUID's loop is 50 nm. **(a)** $a = 50nm$. **(b)** $a = 10nm$

YBCO films on MgO bicrystal substrates with a 24-degree misorientation angle. We use photolithography to define coarse structures, followed by Ar ion milling. Subsequently, FIB with 30 keV Ga ions in a dual beam Focused Ion Beam (FIB) system patterned the selected bridges into nanoSQUIDs[20,22,23]. We obtained a SQUID device with a 220 nm × 380 nm hole. Figure. 7 presents an SEM image of a YBCO nanoSQUID on a MgO bicrystal. Slightly enhanced white noise level down to $S_{\phi}^{1/2} = 175n\Phi_0/\sqrt{Hz}$ [16], we have made an improvement of the sensitivity of this nano-SQUID devices down to the level of single spin sensitivity, which agrees well with our simulation result.

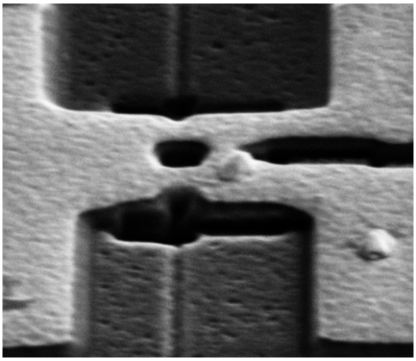

Figure 7. SEM image of a YBCO nanoSQUID on a MgO bicrystal substrate.

4. Conclusion

We illustrated the schemes of a nano-SQUID's detection capability according to the device's geometry and fabrication process. We demonstrated that the performance of the nano-device increased by decreasing the loop size of the SQUIDs, and it reached the maximum value at the corners of the loop. We estimated the flux noise S_Φ of the SQUIDs in the thermal white noise regime and found S_Φ is linearly dependent on the side length and film thickness of the nano-SQUID. We found that the field amplification factor around the cross-section area increases when shrinking the width of the cross-section area of the SQUID loop. We have successfully produced the YBCO-based nano-SQUIDs with Josephson junctions at MgO biocrystal grain boundaries. The spin sensitivity evaluated by the experimentally fabricated devices is comparable with our estimation.

5. Acknowledgment

This work was supported by the National Natural Science Foundation of China (Grant No. 12104112), the Natural Science Foundation of Shandong Province (Grant No. $ZR2021QA036$), and the Fundamental Research Funds for the Central Universities ($3072022TS2602$ and $79000012/011$).

References

[1] John Clarke and Alex I. Braginski. *The SQUID handbook. Vol. 1. Fundamentals and technology of SQUIDs and SQUID systems.* Wiley-VCH, Weinheim, 2004.

[2] Carmine. Granata, Antonio. Vettoliere, P. Walke, C. Nappi, and M. Russo. Performance of nano superconducting quantum interference devices for small spin cluster detection. *Journal of Applied Physics*, 106(2), 2009.

[3] John Clarke and Alex I. Braginski. *The SQUID Handbook Vol II: Applications of SQUIDs and SQUID Systems*. Wiley-VCH, Weinheim, 2004.

[4] Robert Fagaly. Superconducting quantum interference device instruments and applications. *Review of Scientific Instruments*, 77:101101–101101, 2006.

[5] W. Wernsdorfer, D. Mailly, and A. Benoit. Single nanoparticle measurement techniques. *Journal of Applied Physics*, 87(9):5094–5096, 2000.

[6] M. M. Khapaev, M. Yu Kupriyanov, E. Goldobin, and M. Siegel. Current distribution simulation for superconducting multi-layered structures. *Superconductor Science and Technology*, 16(1):24–27, 2002.

[7] Vincent. Bouchiat. Detection of magnetic moments using a nano-squid: limits of resolution and sensitivity in near-field squid magnetometry. *Superconductor Science and Technology*, 22(6):064002, 2009.

[8] Yue Wu, Liye Xiao, Shizhong Hou, Zhaoshun Gao, and Li Han. High tc tmr-superconducting mixed sensor: Fabrication and performance. *IEEE Transactions on Applied Superconductivity*, 29(1):1–5, 2019.

[9] P. F. Vohralik and S. K. H. Lam. Nanosquid detection of magnetization from ferritin nanoparticles. *Superconductor Science and Technology*, 22(6):064007, 2009.

[10] Aico G. P. Troeman, Hendrie Derking, Bert Borger, Johannes Pleikies, Dick Veldhuis, and Hans Hilgenkamp. Nanosquids based on niobium constrictions. *Nano Letters*, 7(7):2152–2156, 2007.

[11] S. Lam and David Tilbrook. Development of a niobium nanosuperconducting quantum interference device for the detection of small spin populations. *Applied Physics Letters*, 82:1078–1080, 2003.

[12] Natalia Sergeeva-Chollet, Hadrien Dyvorne, Hedwige Polovy, Myriam Pannetier-Lecoeur, and Claude Fermon. *Magnetoresistive Hybrid Sensors for Simultaneous Low-Field MRI and Biomagnetic Measurements*, volume 28, pages 70–73. 2010.

[13] Dieter Koelle. A tip for better sensing. *Nature Nanotechnology*, 8(9):617–618, 2013.

[14] J. Nagel, A. Buchter, F. Xue, O. F. Kieler, T. Weimann, J. Kohlmann, A. B. Zorin, D. Rüffer, E. Russo-Averchi, R. Huber, P. Berberich, A. Fontcuberta i Morral, D. Grundler, R. Kleiner, D. Koelle, M. Poggio, and M. Kemmler. Nanoscale multifunctional sensor formed by a ni nanotube and a scanning nb nanosquid. *Physical Review B*, 88(6):064425, 2013.

[15] Silvia Ruffieux. High-temperature superconductingmagnetometers for on-scalp meg. 2020.

[16] Lin Jianxin, Benedikt Müller, Julian Linek, Max Karrer, M. Wenzel, María José Martínez-Pérez, Reinhold Kleiner, and Dieter Koelle. $YBa_2Cu_3O_7$ nano superconducting quantum interference devices on mgo bicrystal substrates. *Nanoscale*, 2020.

[17] Carmine Granata and Antonio Vettoliere. Nano superconducting quantum interference device: A powerful tool for nanoscale investigations. *Physics Reports*, 614:1–69, 2016.

[18] Ling Hao, J. Macfarlane, J. C. Gallop, David Cox, J. Beyer, Dietmar Drung, and T. Schurig. Measurement and noise performance of nano-superconducting-quantum-interference devices fabricated by focused ion beam. *Applied Physics Letters*, 92:192507–192507, 2008.

[19] S. Lam. Noise properties of squids made from nanobridges. *Superconductor Science and Technology*, 19:963, 2006.

[20] Giuseppe C. Tettamanzi, Christopher I. Pakes, Simon K. H. Lam, and Steven Prawer. Flux noise in ion-implanted nanosquids. *Superconductor Science and Technology*, 22(6):064006, 2009.

[21] M. Pannetier, C. Fermon, G. Le Goff, J. Simola, E. Kerr, and J. M. D. Coey. Noise in small magnetic systems—applications to very sensitive magnetoresistive sensors. *Journal of Magnetism and Magnetic Materials*, 290-291:1158–1160, 2005.

[22] J. P. Cleuziou, W. Wernsdorfer, V. Bouchiat, T. Ondarçuhu, and M. Monthioux. Carbon nanotube superconducting quantum interference device. *Nature Nanotechnology*, 1(1):53–59, 2006.

[23] C. P. Foley and H. Hilgenkamp. Why nanosquids are important: an introduction to the focus issue. *Superconductor Science and Technology*, 22(6):064001, 2009.